2025 24th IEEE Intersociety Conference on Thermal and Thermomechanical Phenomena in Electronic Systems (ITherm) | 979-8-3315-2428-9/25/$31.00 ©2025 IEEE | DOI: 10.1109/ITherm55376.2025.11235805

Development of Liquid Metal and Silicon Pin Fin Composite Thermal Interface Materials

Matthew Coughlin[a*], Andrew Clements[a*], Fangzhou Wang[a*], Luke Gyubin Min[a], Kaiying Jiang[a], Heungdong Kwon[a], Mehdi Asheghi[ab], Kenneth Goodson[ac]
[a]*Mechanical Engineering Department, Stanford University, Stanford, CA, 94305 USA*
[*]*Equal contributors*
[b]Masheghi@stanford.edu, [c]Goodson@stanford.edu

***Abstract*—The next generation of high heat flux electronics demand thermal interface materials (TIMs) that balance excellent thermal conductivity with mechanical compliance. This paper focuses on the fabrication and characterization of silicon pin fin and liquid metal (PFLM) composites with target thermal resistance of 1 mm^2KW^{-1}. We micropatterned silicon pin fin wicks (55 µm thickness, 41-96% porosity, 1×1 cm footprint) infiltrated with liquid metal (LM). We utilized high spatial resolution IR cross-sectional microscopy to map the temperature profile, achieving measurement sensitivity of less than 1 mm^2KW^{-1}. To quantify variability between TIMs due to assembly and copper-gallium interfacial reactions, we stacked three PFLM composite samples for each measurement. We measured thermal resistances from 2.2±0.8 mm^2KW^{-1} (41% LM-59% Si) to 5.2±0.9 mm^2KW^{-1} (96% LM-4% Si). The results are in good agreement with a one-dimensional (1D) conduction model and mark a reduction of up to a third from a 51 µm thick LM TIM without pin fins (3.25±1.24 mm^2KW^{-1}). We further show the pin fins precisely control the thickness of the LM. Future work should focus on optimizing the pin fin geometry and making the TIMs resistant to gallium corrosion.**

I. Introduction

The demand to sustain an exponential growth in computing power in microelectronics drives a surge in energy consumption that requires high-performance cooling systems [1-2]. Thermal interface materials (TIMs) are critical for heat dissipation in traditional electronics packages as they provide a low-resistance pathway between the silicon die and heat sink [3]. As semiconductor heat output rapidly approaches 1 $kWcm^{-2}$, the continued use of conventional TIMs such as thermal grease is limited by low conductivity of ~1-4 $W(mK)^{-1}$ [4-5]. The next generation of TIMs must provide improved thermal performance while maintaining elasticity to mitigate stress from thermal expansion and compliance to fill interface cavities [5].

Gallium-based liquid metal (LM) displays a synergy of metallic and liquid properties that make it a promising next-generation TIM. The manufacturer of the eutectic alloy $Ga_{66.5}In_{20.5}Sn_{13}$ reports both excellent thermal conductivity of 16.5 $W(mK)^{-1}$ and low viscosity of 2.4 mPa·s. However, LM TIMs come with limitations. In recent work by Jiang [6], the thickness of the LM was unknown, leading to a variable thermal resistance. Shear interaction between the LM and joining surfaces also limited the minimum thickness of the TIM to an estimated 23 µm, which corresponds to a resistance of 1.4 mm^2KW^{-1}. This was on the same order of magnitude as the theoretical resistance of the material measured in the study (1.3 mm^2KW^{-1}), limiting the sensitivity of the measurement. The present work seeks to address both challenges by fabricating and characterizing composite TIMs made from silicon pin fin wicks infiltrated with LM.

Kim [7] previously fabricated elastic and electrically conductive pin fin and liquid metal (PFLM) composites (10–25 µm thickness, coverage over 1 cm^2) by wicking LM into an array of silicon pin fins. Importantly, the LM thickness was uniform to 0.5 µm. In this work, we studied PFLM composites with a 1x1 cm footprint and 55 µm thickness. The addition of microfabricated pin fins enhances TIM performance by controlling LM placement and establishing a high-conductivity pathway across the composite. At ~140 $W(mK)^{-1}$, the conductivity of silicon is nine times larger than the reported conductivity of LM (16.5 $W(mK)^{-1}$).

After fabrication, we measured PFLM thermal resistance in a modified TIM tester with high sensitivity (±~0.5 mm^2KW^{-1}). Owing to a low theoretical resistance of ~1 mm^2KW^{-1}, characterizing the TIMs according to the popular ASTM D5470 standard is impractical because uncertainty in the measurement (~10 mm^2KW^{-1}) is ten times larger than the resistance of the TIM [8]. Instead, we build on the work of Jiang [6] to make measurements with non-contact infrared (IR) microscopy, attaining sensitivity below 1 mm^2KW^{-1}. The results demonstrate that pin fins control the thickness of the LM and lower resistance by up to a third when compared to LM TIMs. Together, they provide a strategy to bolster the adoption of LM as a TIM in high heat flux electronics.

This work was supported by the National Science Foundation Engineering Research Center for Power Optimization of Electro Thermal Systems (POETS), sub-award number 073708-14989/Award Number: EEC-1449548. Part of this work was performed at the Stanford Nanofabrication Facility (SNF) and Stanford Nano Shared Facilities (SNSF), supported by the National Science Foundation under award ECCS-2026822. M. C. and A. C. are supported by the National Science Foundation Research Experience for Undergraduates award number EEC-1659794. L. G. M. is supported by the Stanford Graduate Fellowship.

II. Methodology

A. Pin fin and liquid metal (PFLM) TIM preparation

Jiang [6], Ji [9], and Yan [10] previously created LM TIMs on a flat substrate. The process to fabricate PFLM TIMs is a direct modification to the methodology in [6], so we include a discussion of that process and its limitations in the appendix.

We address the shortcomings of LM TIMs by patterning an array of pin fins on a Si substrate. The pin fin diameter d, edge-to-edge spacing l, and thickness t dictate the thermal resistance, manufacturability, and wettability of the TIM. With proper spacing and density, the pin fins act as a wick which spreads the LM into a thin, uniform film. Kim [7] used the Wenzel model to predict the wettability of pin fin geometries. We use the same model here to select the parameters d and l to attain TIMs with porosity spanning from 41-96%. The thickens of all samples was constant at $t = 55$ µm. The appendix includes a discussion of pin fin geometry selection.

The complete fabrication process for PFLM chips is documented in (Fig. 1), and the colors for each material are presented in Table 1. The most important change from the flat substrate case comes in (Fig. 1a), when pin fins are etched into the Si wafer using deep reactive ion etching (DRIE). The etching process provides precise control over pin fin geometry, with uncertainty in diameter and spacing below 1 µm. After etching, the height of the pin fins was verified with a thickness gauge. All geometries fell within $t = 55 \pm 4$ µm.

A large contact angle prevents LM from wetting non-metallic surfaces, including Si [7]. To overcome this limitation, we sputter-deposit a Cu film on the Si wafer (Fig. 1b). The Cu promotes LM imbibition through a reactive wetting process. However, a native oxide layer (Ga_2O_3/Ga_2O) forms on the LM ($Ga_{66.5}In_{20.5}Sn_{13}$) in air, inhibiting wetting. The wetting is performed in a 3M HCl solution (Fig. 1c) to remove the oxide layer.

We optically verify wetting by observing the transition from Cu- to LM-covered pin fins. (Fig. 2d) shows LM wicking into the pin fin array, which takes about 5 minutes. Then, the PFLM chip is pressed against the backside of a joining wafer to create the TIM. This compression stage (Fig. 2f) highlights a key benefit of the pin fins, as they control the thickness of the LM layer.

TABLE I. Material Color Code for Figures

Material	Application
Cu	Metal coating on Si wafer to facilitate LM wetting or cooler block in TIM tester
Si wafer	Substrate and pin fin material
Liquid metal (LM)	Liquid component of PFLM TIM
PFLM TIM	High performance TIM
Pt heater	Heater on the back of one PFLM TIM
Silicone rubber	Insulation in TIM tester
Kapton tape	Spacer in LM TIM without pin fins

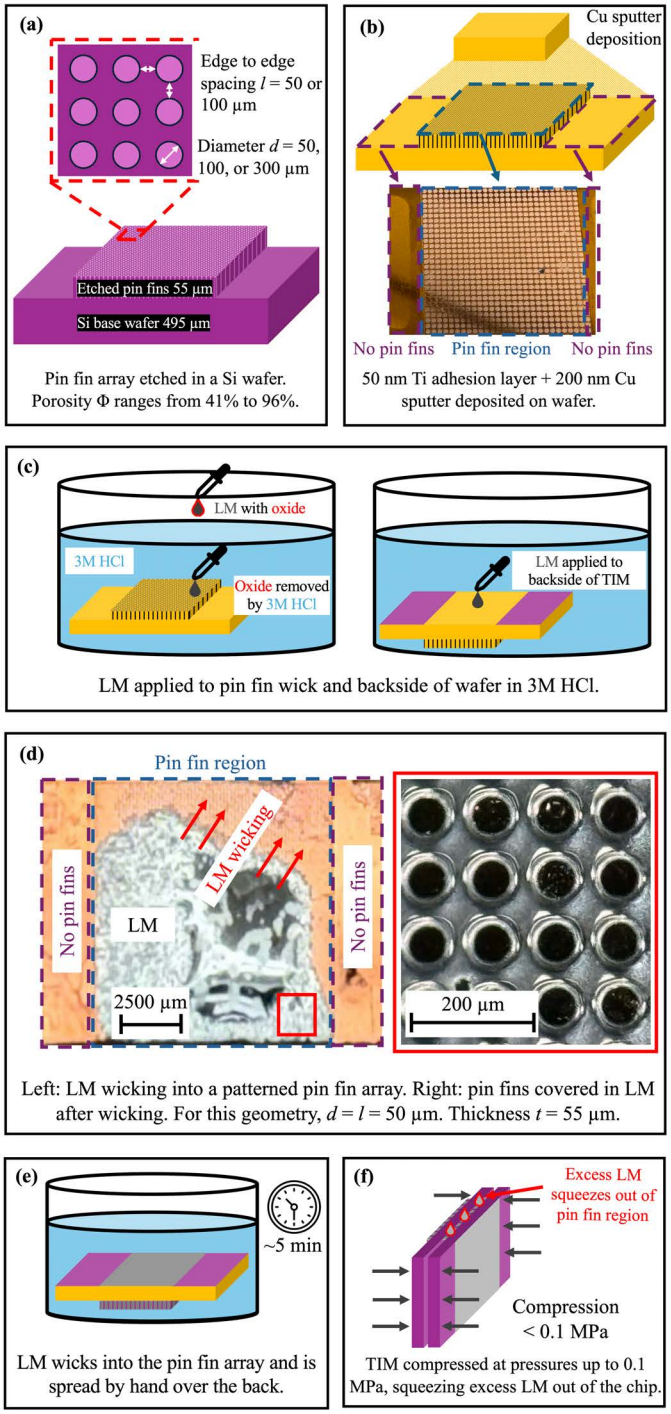

Fig. 1. Fabrication and assembly process for PFLM TIMs. (a) pin fins etched into a 550 µm Si wafer with deep reactive ion etching (DRIE). Pin fin geometries: porosity Φ = 41% (d = 300 µm; l = 50 µm), Φ = 66% (d = 100 µm; l = 50 µm), Φ = 80% (d = 50 µm; l = 50 µm), and Φ = 96% (d = 30 µm; l = 100 µm). (b) sputter coating of 50 nm Ti and 200 nm Cu. The metal film is necessary for reactive wetting. (c) Wicking of LM performed in 3M HCl solution. HCl removes the oxide layer (Ga_2O_3/Ga_2O) from the LM droplet. LM is added to the pin fin array and the matching area on the back of the wafer, which is also covered by the Cu film. (d) Left: LM wicking into the pin fin array, showing a clear delination between region wet with LM (gray) and not wet (orange). Right: LM coats all surfaces of the pin fins. (e) LM wetting takes ~5 minutes in 3M HCl. (f) TIM assembled by compressing pin fin region into LM-coated backside of the joining Si wafer. Pressures applied during assembly are <0.1 MPa, which is sufficient to squeezes excess LM out of the pin fin wick.

B. PFLM TIM characterization

Computing the thermal resistance of a TIM according to the conventional ASTM D5470 standard requires using thermocouples to measure the temperature profile in two reference blocks. However, variability in thermocouple placement leads to uncertainty as high as 10 mm^2KW^{-1} [8], which is close to an order of magnitude above the theoretical resistance of the PFLM TIMs. To improve measurement sensitivity for TIMs with a resistance of ~1 mm^2KW^{-1}, Jiang [6] used high spatial resolution IR microscopy. We adopt a similar approach in the current work, recording the temperature profile with a QFI InfraScope II operating at 5x magnification (spatial resolution ~4.5 µm/pixel). A schematic of the TIM tester is presented in (Fig. 2).

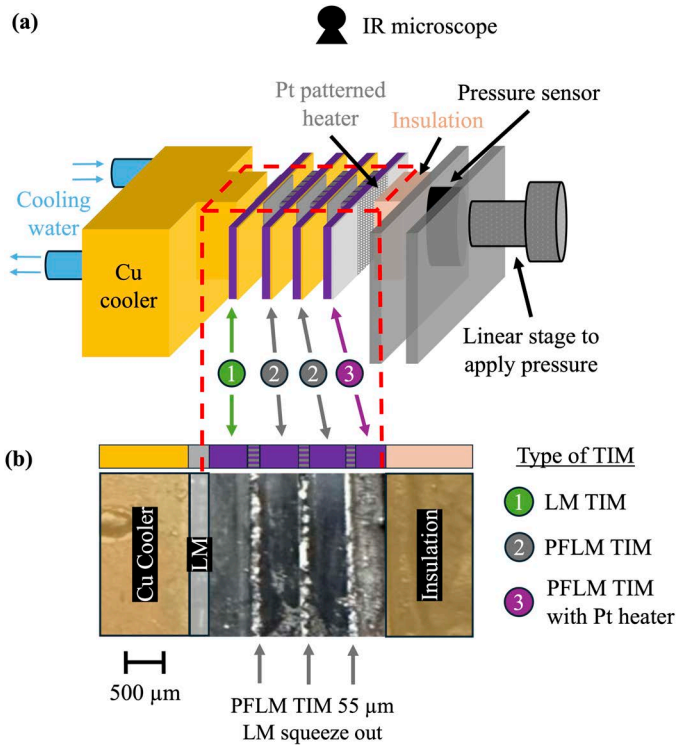

Fig. 2. The TIM tester used for PFLM characterization. (a) Heat is applied to the PFLM TIMs by a patterned mesh heater (50 nm Ti + 100 nm Pt) on the backside of the first wafer. Each measurement includes two PFLM TIM chips stacked together. One LM TIM is placed at the cooler interface to ensure the roughness of the surface connected to each PFLM TIM is constant. (b) An optical image of the surface of the TIMs facing the IR microscope. The surface is painted black to increase emissivity. Lines of excess LM squeezing out of the TIM labeled.

The high resolution IR microscope allows for precisely finding the temperature drop across a TIM. However, computing the resistance also requires knowing the heat flux through the sample. In Jiang's work in [6], the heat flux was calculated from the temperature profile in the Si wafer using (1):

$$q'' = k\frac{dT}{dx} \quad (1)$$

where q" is the heat flux, $\frac{dT}{dx}$ is the temperature gradient in the Si wafer, and k is the thermal conductivity of Si. However, this approach is sensitive to noise in the temperature profile. To minimize uncertainty, we patterned a mesh heater (50 nm Ti + 100 nm Pt) with the same 1 cm^2 footprint of the PFLM TIM on the backside of one Si wafer. This generates a uniform, one-dimensional heat flow, allowing us to calculate the heat flux from the power supplied to the heater using (2):

$$q'' = \frac{V \times I}{A} \quad (2)$$

where q" is the heat flux, V is the voltage difference across the heater, I is the current through the heater, and A is the area of the TIM. Insulation (silicone rubber, ~0.1 $W(mK)^{-1}$) prevents heat loss from the backside.

A traditional ASTM D5470 TIM tester measures one TIM at a time. However, for maximum sensitivity, the resistance of the TIM region should dominate the total thermal resistance of the tester. In our apparatus, the cooler surface is sanded copper, leading to a resistance of ~20 mm^2KW^{-1} at the interface. To increase the total resistance of the TIM region to be comparable with the cooler interface, three PFLM chips are measured simultaneously. To maintain consistent surface properties at all PFLM TIM interfaces, a Si wafer sputter-coated with Cu is placed between the last TIM and the Cu cooler.

The temperature of the cooler was maintained at 50±0.1 °C by a water chiller (Neslab, RTE-7). A linear displacement stage (HR-13 High-Resolution Micrometer Head) applied pressure to the sample, which was measured by a load cell (TE Connectivity, FC2231). The maximum pressure for the load cell was 0.4 MPa. The IR microscope recorded temperature data in the region indicated by a red box in (Fig. 2a) and pictured in (Fig. 2b). The surfaces facing the IR camera were covered with black paint (emissivity ~0.94) to increase the sensitivity of the IR measurement.

III. Results and Discussion

A. Thermal resistance measurement

(Fig. 3) presents a representative temperature profile from a TIM characterization experiment. A block diagram in (Fig. 3a) clarifies the location of each PFLM TIM.

We measured the temperature across the exposed surface of the TIMs using an IR microscope and present a representative result in (Fig. 3b). The temperature is nearly uniform along the width of the TIM (the *y*-direction in Fig. 3), so the temperature profile can be treated as one-dimensional. For all subsequent analysis, we obtain a one-dimensional profile by averaging along the *y*-direction.

(Fig. 3c) shows the temperature profile after averaging. Each TIM displays a linear regime in the base Si substrate and a sharp drop at the interface. Computing the thermal resistance requires extracting the temperature drop across the TIMs. Small non-linearities at the interface, attributed to excess LM squeezing out of the TIM, prevent us from measuring the temperature drop dT_{PFLM} directly. Instead, we extrapolate the linear profile in the Si substrates to the interface.

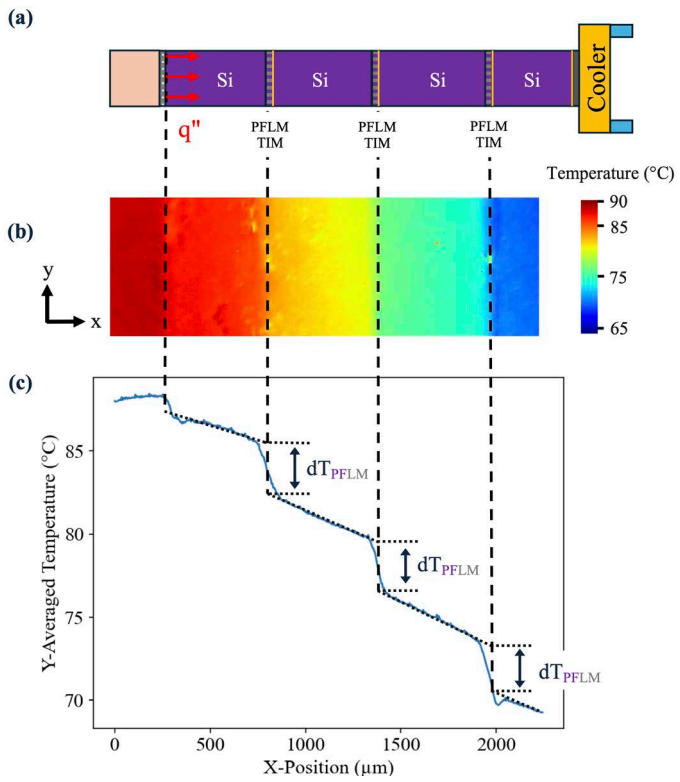

Fig. 3. Results of a thermal resistance measurement for PFLM TIMs with 80% porosity. (a) Diagram of the TIM tester with PFLM TIM interfaces labeled. (b) IR image of the TIM tester. (c) *Y*-averaged temperature profile of the TIM tester. Each sample displays a linear regime in the Si wafer and a sharp drop across the TIM. Temperature drops across the TIM, labeled as dT_{PFLM}, are calculated by extrapolating the linear temperature profile to the interface.

Computing thermal resistance also requires calculating the heat flux from the power supplied to the patterned heater. For the data in (Fig. 3), the heat flux is 109.2±0.11 Wcm^{-2}. From the heat flux and temperature drop, the TIM resistance can be computed using (3):

$$R''_{PFLM} = \frac{dT_{PFLM}}{q''} \quad (3)$$

where R''_{PFLM} is the resistance of the TIM, dT_{PFLM} is the temperature drop across the material, and q" is the heat flux. For the three 80% porosity PFLM TIMs shown in (Fig. 3), the resistance is 2.85 mm^2KW^{-1} with measurement uncertainty of ±0.59 mm^2KW^{-1} and random variability between TIMs of ±0.25 mm^2KW^{-1}. The measurement uncertainty is only 20% of the resistance, demonstrating that the IR microscope and patterned heater allow for sensitive TIM characterization. A full discussion of the uncertainty calculation is reserved for the appendix.

B. Dependency of thermal resistance on pressure

In PFLM TIMs, the Si pin fins control the thickness of the liquid metal by providing mechanical strength to fix the distance between the joining substrates. To probe how effectively the pin fins control LM thickness, we measured the TIM resistance at pressures of 0.1, 0.25, and 0.4 MPa. A measurement far above the maximum pressure of our sensor was also recorded by hand-tightening the linear stage as far as possible. This pressure is reported as "high." Representative data is included in (Fig. 4).

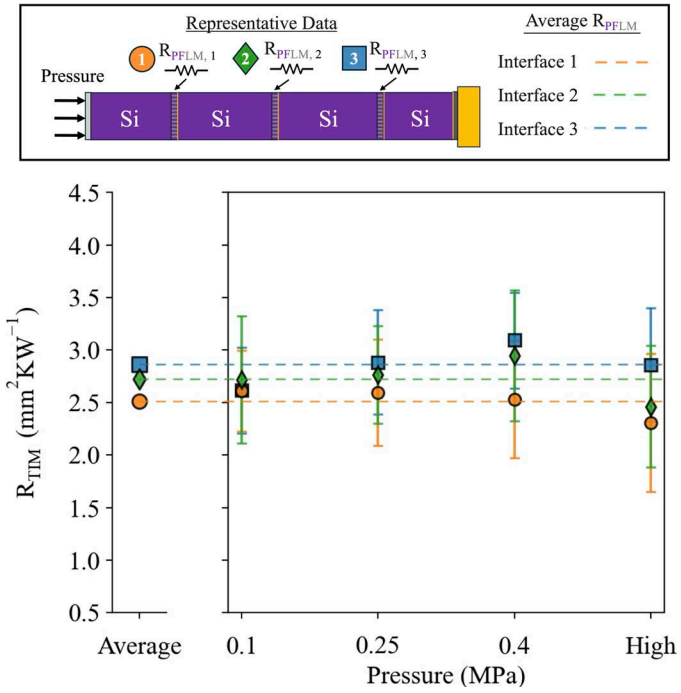

Fig. 4. Representative data showing the resistance of three 80% porosity PFLM TIMs as a function of pressure. Each TIM in the tester is represented by a unique marker (●, ♦, ■). Error bars show measurement sensitivity. The resistance is independent of pressure.

The thermal resistance of the TIMs shows no discernable dependance on pressure. From this observation, we conclude that the thickness of the LM in the TIM is constant, since any change in thickness results in a change in resistance using (4):

$$R''_{PFLM} = \frac{t}{k_{TIM}} \quad (4)$$

where t is the thickness of the TIM and k_{TIM} is the effective thermal conductivity of the material. We also observe that LM squeezes out of the TIMs during assembly as pressure is increased from 0 to 0.1 MPa, but the squeeze-out stops by 0.1 MPa, which further supports this conclusion. The results collectively demonstrate that the pin fins precisely control the thickness of the LM at pressures above 0.1 MPa, an objective of the present work.

C. *Dependance of thermal resistance on pin fin geometry*

Pin fins and LM serve different roles in dictating the thermal performance of the composite TIM. The pin fins provide a high conductivity pathway for heat flow, while LM fills interfacial air pockets at the interfaces. In search of the optimal TIM geometry, we vary the porosity of the composite. (Fig. 5) below shows the thermal resistance of the PFLM TIMs as a function of porosity.

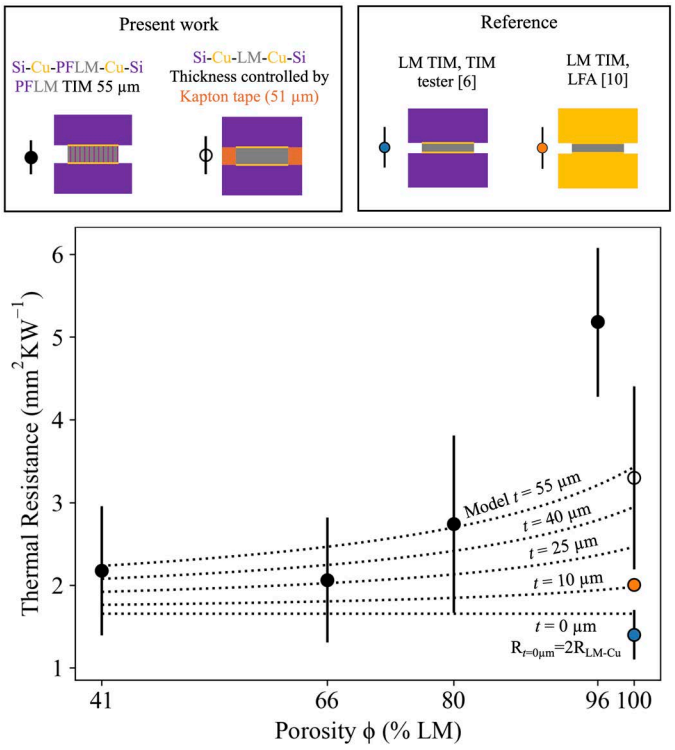

Fig. 5. Thermal resistance of PFLM TIMs ( ) across four porosities. Three baseline measurements on a smooth surface without pin fins are included. A 51 µm LM TIM with thickness controlled by Kapton tape (, present work) provides a comparison with the PFLM TIMs, as they are nearly the same thickness. We also include values from the literature for a LM TIM with uncontrolled thickness measured in a TIM tester ( ) [6] and a 2.5 µm LM TIM characterized by LFA ( ) [10] to provide a lower limit to reported LM TIM performance. A 1D conduction model is also plotted to show the theoretical performance of the PFLM TIMs at various thicknesses. Model parameters k_{LM} and $R_{LM\text{-}Cu}$ measured from the 51 µm LM TIM data.

To act as a baseline for our results, (Fig. 5) includes the thermal resistance of a 51 µm LM TIM, which is nearly the same thickness as the 55 µm PFLM TIMs. Kapton tape was used to create a thin gap between two Cu-coated Si wafer, which we filled with LM. At 3.25±1.24 mm^2KW^{-1}, the baseline is up to 1 mm^2KW^{-1} higher than the resistance of the 41%, 66%, and 80% porosity TIMs, confirming that PFLM TIMs perform better than LM TIMs on a flat substrate.

We also compare our results with literature values for LM films, the highest-performing conventional LM TIMs. Jiang [6] sandwiched LM between two Cu-coated Si wafers at pressures up to 1 MPa and reported a thermal resistance of 1.4±0.3 mm^2KW^{-1} with no dependance on pressure. Yan [10] took a different approach, measuring the resistance of a LM film with an estimated thickness of 2.5 µm with laser flash analysis. Both resistances are lower than the PFLM TIMs, which we attribute to the smaller thickness. In future work, pin fin thickness should be decreased to further improve the PFLM TIM performance.

To predict the theoretical performance of the TIMs, we constructed a simple thermal circuit by treating the LM and pin fins as two resistances in parallel. (Fig. 6) below shows the model:

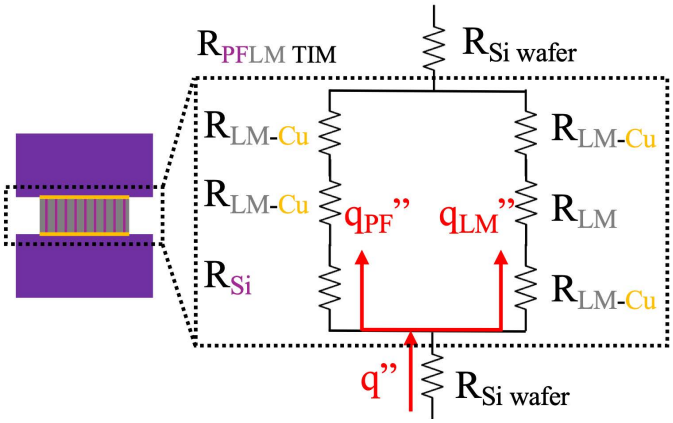

Fig. 6. A one-dimensional thermal resistance model for PFLM TIMs. The path on the left represents the pin fins, and the path on the right corresponds to the LM. We treat the pin fins and adjacent wafer as though they are joined by a LM film with negligible thickness. At 200 nm, the resistance of the Cu film is negligible (~$5x10^{-4}$ mm^2KW^{-1}).

The model in (Fig. 6) yields (5):

$$R_{PFLM} = \frac{t}{\phi\, k_{LM} + (1-\phi)k_{Si}} + 2R_{LM\text{-}Cu} \qquad (5)$$

where k_{Si} and k_{LM} are the thermal conductivity of Si and LM, respectively, ϕ is the porosity of the composite, and $R_{LM\text{-}Cu}$ is the thermal boundary resistance between LM and Cu. From the baseline 51 µm LM TIM, we calculate k_{LM} as 31±1 $W(mK)^{-1}$ and $R_{LM\text{-}Cu}$ as 0.76±0.1 mm^2KW^{-1}. A discussion of the calculation is included in the appendix. These results are near literature values for LM thermal boundary resistance of 0.974 mm^2KW^{-1} [10] and k_{LM} of 28.1±3.5 $W(mK)^{-1}$ [11].

The one-dimensional conduction model and experimental results are in good agreement. Both show PFLM TIM resistances spanning 2 to 3 mm^2KW^{-1} with resistance gradually increasing with porosity. The contribution from the bulk resistance of the PFLM layer diminishes with decreasing TIM thicknesses. In the most extreme case, at thickness $t = 0$ µm, the resistance is independent of porosity, when the TIM is modeled as two Cu-coated Si wafers joined through wet contact by a LM film of infinitesimal thickness. This results in a resistance of $2R_{LM\text{-}Cu}$ = 1.52±0.2 mm^2KW^{-1}, which is in good agreement with Jiang's measurement of a LM film (1.4±0.3 mm^2KW^{-1}) [6]. The agreement between model and results confirms that adding Si pin fins to a LM TIM enhances heat transfer across the composite.

However, the experimental results come with limitations, including an outlier at 96% porosity and high variability in thermal resistance between PFLM TIMs with identical geometry. After characterizing six 80% porosity PFLM TIMs, we report a resistance of 2.74±1.07 mm^2KW^{-1}, with 20% of this

uncertainty attributed to the instruments and 80% caused by variation between PFLM TIMs. To investigate the root cause of the high TIM-to-TIM variability, we inspect the TIMs after characterization. (Fig. 7) presents the results.

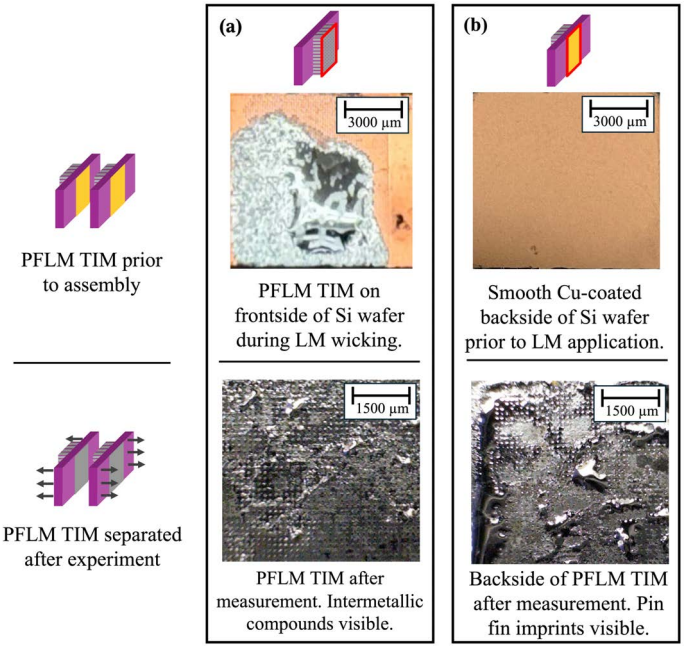

Fig. 7. PFLM TIM before assembly (top row) and after a characterization measurement (bottom row). (a) Pin fin wick etched into a Si wafer. Prior to TIM assembly, the LM is light gray and reflective. After a measurement, the surface is covered by LM droplets and a new compound. (b) The new compound also appears on the joining surface. Note the imprints of pin fins are visible, confirming that the pin fins control LM thickness.

On application, the LM is a smooth, reflective liquid (top row in Fig. 7a). However, inspecting the PFLM TIM after characterization reveals a dull gray compound covering the pin fin wick and joining wafer (bottom row Fig. 7). We believe this compound is a copper-gallium intermetallic ($CuGa_2$/Cu_9Ga_4). Most investigations into Cu-Ga interfacial interactions take place at higher temperature (>150°C) or longer time (> 3h) than our experiments [12], which occur below 100°C and last ~1h. This makes it challenging to predict the formation of the compounds or estimate the impact on the thermal resistance of the TIM. However, we observe the area of the pin fin wick covered by LM upon disassembly ranges from ~20-80%, which may contribute to the high experimental variability. In future work, the Cu layer should be replaced with a non-reactive metal to prevent the formation of intermetallic compounds.

IV. Conclusion

This study details the fabrication and characterization of PFLM TIMs. Pin fins control the geometry of the LM film and reduce the thermal resistance of the composites. We measured the resistance of PFLM TIMs with porosity between 41% and 96%, reporting resistances as low as 2.06±0.76 mm^2KW^{-1} for the geometry with 66% porosity and as high as 5.18±0.9 mm^2KW^{-1} for the geometry with 96% porosity. Importantly, the resistance of 2.06±0.76 mm^2KW^{-1} is more than 1 mm^2KW^{-1} below the resistance of a 51 µm LM TIM without pin fins, making PFLM composites an attractive TIM for high heat flux applications. However, the TIMs suffered from high variability between samples of ~1 mm^2KW^{-1}, which we attribute to the formation of intermetallic compounds at the LM-Cu interface. In future work, the Cu coating on the Si wafer should be replaced with a metal that resists gallium corrosion. The collective results demonstrate a promising next-generation TIM with applications in thermal management for high heat flux electronics and provide an exciting direction for the use of liquid metal TIMs.

Acknowledgments

M.C. and A. C. thank Tracy Dace, Jodi Gritten, and John Wierschem for organizing the POETS REU program.

References

[1] E. Laloya, Ó. Lucía, H. Sarnago, and J. M. Burdío, "Heat Management in Power Converters: From State of the Art to Future Ultrahigh Efficiency Systems," IEEE Transactions on Power Electronics, vol. 31, no. 11, pp. 7896–7908, 2016, doi: 10.1109/TPEL.2015.2513433.

[2] S. Salahuddin, K. Ni, and S. Datta, "The era of hyper-scaling in electronics," Nature Electronics, vol. 1, no. 8, pp. 442–450, Aug. 2018, doi: 10.1038/s41928-018-0117-x.

[3] K. M. Razeeb, E. Dalton, G. L. W. Cross, and A. J. Robinson, "Present and future thermal interface materials for electronic devices," International Materials Reviews, vol. 63, no. 1, pp. 1–21, 2018, doi: 10.1080/09506608.2017.1296605.

[4] A. Bar-Cohen, J. J. Maurer, and A. Sivananthan, "Near-Junction Microfluidic Cooling for Wide Bandgap Devices," MRS Advances, vol. 1, no. 2, pp. 181–195, Jan. 2016, doi: 10.1557/adv.2016.120.

[5] V. Zhirnov et al., "Microelectronics and Advanced Packaging Technologies Roadmap," Semiconductor Research Corporation, Durham, North Carolina, United States, 2023.

[6] K. Jiang et al., "High-Precision Thermal Characterization of Ultra-Low Thermal Resistance Copper Nano-Wire (CuNWs)-Polydimethylsiloxane (PDMS) Composite Thermal Interface Materials (TIMs) Tape", ASME 2024 International Technical Conference and Exhibition on Packaging and Integration of Electronic and Photonic Microsystems. 2024, doi: 10.1115/IPACK2024-140287.

[7] J.-H. Kim et al., "Imbibition-induced selective wetting of liquid metal," Nature Communications, vol. 13, no. 1, p. 4763, Aug. 2022, doi: 10.1038/s41467-022-32259-3.

[8] R. J. Warzoha, A. N. Smith, and M. Harris, "Improved methodology for calculating interfacial thermal resistance and uncertainty for steady-state TIM testers with embedded probes," 15th IEEE ITHERM, 2016, pp. 1040–1050. doi: 10.1109/ITHERM.2016.7517662.

[9] Y. Ji et al., "Excellent thermal performance of gallium-based liquid metal alloy as thermal interface material between aluminum substrates," Applied Thermal Engineering, vol. 166, p. 114649, 2020, doi: 10.1016/j.applthermaleng.2019.114649.

[10] H. Yan et al., "Wettability and thermal performance of $Ga_{62.5}In_{21.5}Sn_{16}$ liquid metal alloy on W-coated Cu substrates with varying film thickness," International Journal of Thermal Sciences, vol. 172, p. 107333, 2022, doi: 10.1016/j.ijthermalsci.2021.107333.

[11] K. Jiang et al., "Fabrication and Thermal Characterization of Copper Nanowires (CuNWs) Thermal Interface Materials Tapes," 23rd IEEE ITHERM, 2024, pp. 1–10. doi: 10.1109/ITherm55375.2024.10709516.

[12] S. Liu, K. Sweatman, S. McDonald, and K. Nogita, "Ga-based alloys in microelectronic interconnects: A review," Materials, vol. 11, no. 8, p. 1384, 2018.

APPENDIX

A. Shortcomings of LM TIMs on a flat substrate

PFLM TIMs are a direct improvement to LM TIMs, so we discuss the LM TIM fabrication process and its limitations as a reference. The steps to manufacture a LM TIM from [6] are shown in (Fig. 8).

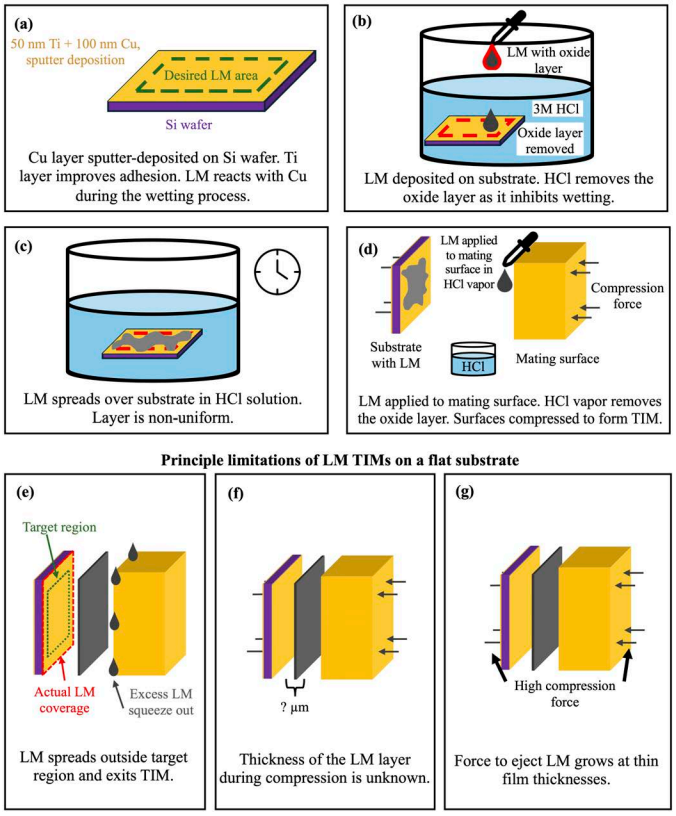

Fig. 8. Limitations of LM TIMs on a flat substrate. (a-d) presents the wetting process. (a) 50 nm Ti + 100 nm Cu are deposited on the Si substrate to facilitate reactive wetting. (b) HCl solution removes the native oxide layer from the LM droplet, enabling the LM to wet the surface. (c) LM spreads over surface in HCl solution. (d) LM is applied to the joining surface in HCl vapor, which removes the oxide layer, and the TIM is compressed. (e-f) highlight the main limitations of the LM TIM. (e) LM covers the full substrate, spreading beyond the target region. (f) Thickness of the LM is unknown, making the thermal resistance of the TIM unknown. (g) A large compression force is required to squeeze the LM into a thin layer.

High surface tension prevents LM from wetting silicon [7], so a Cu layer is deposited on the wafer (Fig. 8a). A native oxide layer (Ga_2O_3/Ga_2O) on the LM also prevents wetting. It is removed using a 3M HCl solution (Fig. 8b). The limitations of LM TIMs become clear in (Fig. 8c), as the LM forms a non-uniform layer on the substrate. Poor control over LM placement is problematic in electronic packages as gallium-based LMs are electrically conductive. Any leakage from the TIM onto a surrounding circuit can trigger a short circuit. (Fig. 8e) shows the LM spreading beyond the target area and squeezing out of the TIM.

The compression stage in (Fig. 8d) is necessary to squeeze the LM into a film, but it introduces two additional challenges. First, as shown in (Fig. 8f), the thickness of the LM layer is uncontrolled, leading to uncertainty in the resistance of the film. Second, as shown in (Fig. 8g), a large compressive force is required to fabricate thin LM TIMs. To drive excess LM out of the film, the applied pressure must overcome the shear force between the LM and substrate, which increases as the gap narrows. However, the maximum applied pressure is limited by the brittle Si wafer.

B. Pin fin geometry selection

The pin fin geometry, determined by the thickness t, diameter d, and edge-to-edge spacing l, dictates the thermal resistance, wettability, and manufacturability of the TIMs. In this study, pin fin height was constant at t = 55 µm. Thinner TIMs offer lower thermal resistance, but this also leads to lower measurement sensitivity. (Fig. 9) presents the four geometries measured in the present work.

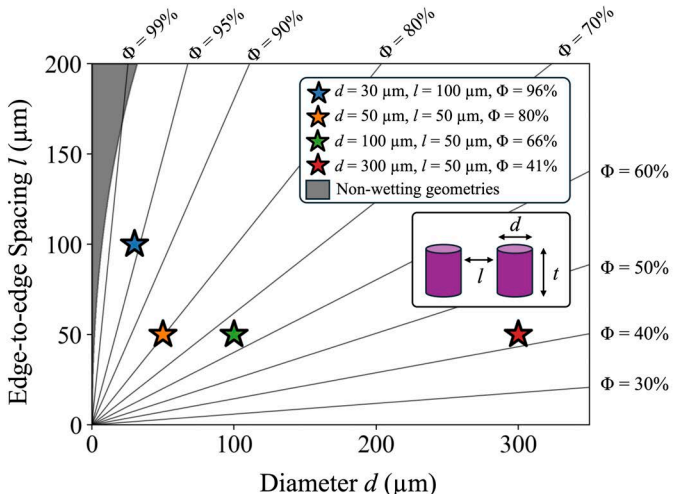

Fig. 9. Pin fin geometries measured in the present work, spanning from Φ = 41% to Φ = 96%. Lines of constant porosity, showing geometries with the same theoretical resistance, are plotted from Φ = 30% to Φ = 99% . The height of the pin fins in the present work is constant at t = 55 µm. The gray region indicates non-wetting geometries.

We use the model proposed by Kim in [7] to demonstrate that all four geometries will act as a wick for LM. With circular pin fins, possible porosities span from 21% to 100%, and the tested geometries fall between porosities of 41% and 96%, spanning close to two-thirds of the full range.

C. LM condcutivity and thermal boundary resistance

The one-dimensional conduction model plotted in (Fig. 5) requires knowing the thermal conductivity of LM and the thermal boundary resistance at a LM-Cu interface. We compute both parameters from the temperature profile in a 51 µm LM TIM without pin fins. (Fig. 10) shows a representative temperature profile across the LM TIM, which closely resembles the profiles observed in PFLM TIMs.

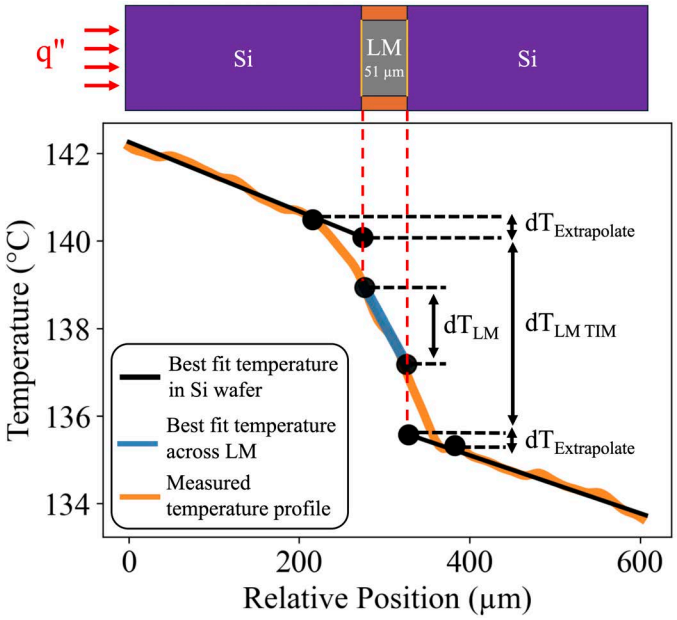

Fig. 10. Representative temperature profile across a 51 µm LM TIM interface. Temperature drops are labeled. The temperature profile closely resembles the results from a PFLM TIM measurement, with a linear profile in the Si wafer and a sharp drop across the TIM. Linear fit for the temperature profile in the LM and Si wafers included.

The IR microscope offers resolution of 4.5 µm/pixel, allowing us to measure 11 data points across the 51 µm thick LM TIM. We extract the temperature gradient in the LM by fitting a line to this data, shown in blue on (Fig. 10). From the heat flux and temperature gradient, the thermal conductivity of the LM can be calculated using (6):

$$k_{LM} = \frac{q''}{dT/dx} \tag{6}$$

This calculation results in a thermal conductivity k_{LM} of 31±1 W(mK)$^{-1}$, which corresponds to a thermal resistance of 1.64±0.05 mm^{2}KW^{-1} for a 51 µm LM TIM. Like the PFLM samples, the temperature profile in the Si substrate is extrapolated to the interface to compute the total resistance of the TIM. By applying a one-dimensional conduction model, the LM-Cu interface resistance can be found using (7):

$$R_{LM-Cu} = \frac{R_{LM\,TIM} - R_{LM}}{2} \tag{7}$$

where $R_{LM\,TIM}$ is the total resistance across the TIM, responsible for the temperature drop $dT_{LM\ TIM}$, and R_{LM} is the bulk resistance of the LM layer. Performing this calculation yields an interface resistance of $R_{LM\text{-}Cu} = 0.76 \pm 0.1$ mm^{2}KW^{-1}.

D. Uncertainty calculations

Using (3), PFLM TIM resistance is calculated by dividing the temperature drop across the TIM by the heat flux. For a general function of two variables, (8) gives the uncertainty.

$$U_f^2 = U_a^2\left(\frac{\partial f}{\partial a}\right)^2 + U_b^2\left(\frac{\partial f}{\partial b}\right)^2 \tag{8}$$

where $f = f(a, b)$ and U_f, U_a, and U_b are the respective uncertainties. Applying (8) to the thermal resistance equation (3) leads to (9) below:

$$U_R = \sqrt{\left(\frac{1}{q''}\right)^2 U_{dT}^2 + \left(-\frac{dT}{q''^2}\right)^2 U_{q''}^2} \tag{9}$$

where q" is the heat flux, dT is the temperature drop across the TIM, and U_R, U_{dT}, and $U_{q''}$ are the respective uncertainties. (Fig. 11) below presents an representative temperature profile of a PFLM TIM interface.

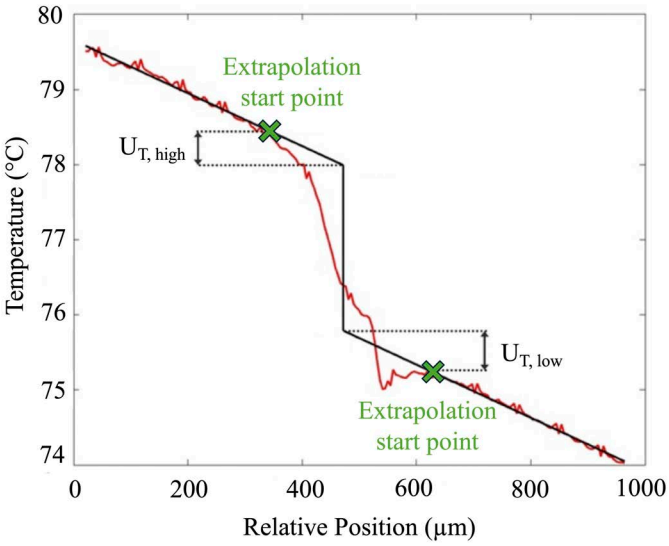

Fig. 11. Enlarged temperature profile near a PFLM TIM. Parameters for the uncertainty analysis labeled.

A conservative estimate for the uncertainty in the extrapolation is the difference between the linear end point temperature and the extrapolated interface temperature, labeled as $U_{T,\,high}$ and $U_{T,\,low}$ on the figure. Both values can be combined to find the uncertainty U_{dT} using (10).

$$U_{dT} = \sqrt{U_{T,\ high}^2 + U_{T,\ low}^2} \tag{10}$$

The uncertainty in heat flux is computed by combining (2) with the uncertainty equation in (8), producing (11):

$$U_{q''} = \sqrt{\left(\frac{1}{A}\right)^2 U_q^2 + q^2 U_A^2} \tag{11}$$

The microfabrication process provides micron-level control over TIM geometry, making the uncertainty in area U_A negligible. U_q can be calculated from the resistor network shown in (Fig. 12).

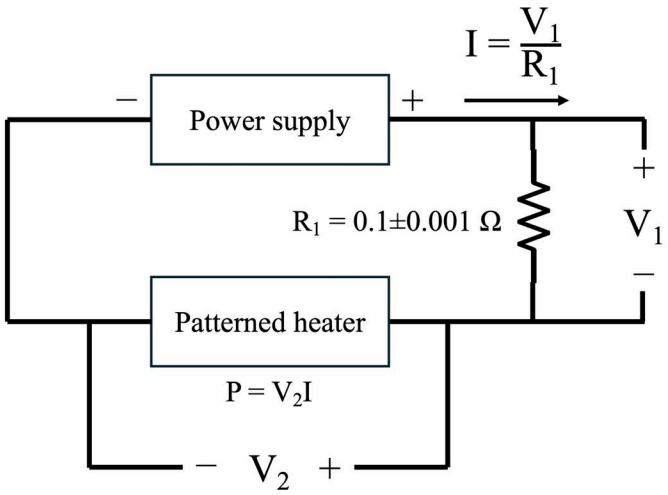

Fig. 12. Electrical diagram for the patterned heater and resistance network. The heat applied to the TIM is calcualted from the current and voltage across the heater.

From (Fig. 12) the uncertainty in heat flux and current can be calculated using (12-13).

$$U_q = \sqrt{V_2^2 U_I^2 + I^2 U_{V_2}^2} \tag{12}$$

$$U_I = \sqrt{\left(\frac{1}{R_1}\right)^2 U_{V1}^2 + {V_1}^2 U_{R1}^2} \tag{13}$$

The high accuracy of the voltmeter makes U_{V1} and U_{V2} negligible. The resistor R_1 is accurate to ±1%, making U_q, low at ~±0.1 Wcm^{-2} for the heat fluxes of ~110 Wcm^{-2} used in the current work. This illustrates a key advantage of the patterned heater, as the uncertainty in thermal resistance due to the heater is ~±0.03 mm^2KW^{-1}, which is small compared to the contribution from the temperature extrapolation of ~±0.5 mm^2KW^{-1}.